Mechanisms underlying the vulnerability of seasonally dry ecosystems to drought

Daniella M Rempe[1,a], Erica L McCormick[1,a], W Jesse Hahm[2], Geeta Persad[1], Cameron Cummins[1], Dana A Lapides[2,3], K Dana Chadwick[1,4], David N Dralle[3]

[1] Jackson School of Geoscience, University of Texas, Austin, Austin, TX, USA

[2] Department of Geography, Simon Fraser University, Burnaby, BC, Canada

[3] Pacific Southwest Research Station, USDA Forest Service, Davis, CA, USA

[4] NASA Jet Propulsion Laboratory, California Institute of Technology, Pasadena, CA 91109

[a] Denotes co-first author

Correspondence to: rempe@jsg.utexas.edu

"

Mechanisms underlying the vulnerability of seasonally dry ecosystems to drought

Daniella M. Rempe[a,*], Erica L. McCormick[a,*], W. Jesse Hahm[b], Geeta Persad[a], Cameron Cummins[a], Dana A. Lapides[b,c], K. Dana Chadwick[a,d], and David N. Dralle[c]

[a]Jackson School of Geoscience, University of Texas at Austin, Austin, TX 78712
[b]Dept of Geography, Simon Fraser University, Burnaby, BC, Canada, V5A 1S6
[c]Pacific Southwest Research Station, United States Forest Service, Davis CA 95618
[d]NASA Jet Propulsion Laboratory, California Institute of Technology, Pasadena CA 91109.
katherine.d.chadwick@jpl.nasa.gov.
[*]D.M.R. contributed equally to this work with E.L.M.

Correspondence: Daniella Rempe (rempe@jsg.utexas.edu)

Abstract.

5   Root-zone water storage (RWS) dynamics regulate when plants experience drought-related water stress and mortality. However, because RWS capacity (S_{max}) is poorly known, it remains challenging to translate variability in precipitation to water stress. Here, we investigate the relationship between precipitation variability and S_{max} and implement a framework for identifying the vulnerability of seasonally dry woody ecosystems to projected climate change. Using novel estimates of S_{max} across California, we demonstrate that where dry-season RWS is routinely capped by S_{max}, plants are less vulnerable to precipitation

10   variability relative to where dry-season RWS varies annually with precipitation. Using direct measurements of RWS and S_{max} at three field sites, we illustrate how these differences in vulnerability arise due to variations in bedrock properties. We calculate that up to 23% of California's total biomass is sensitive to year-to-year variations in precipitation and can experience carryover of moisture from one year to the next. Contrary to the notion that deep weathering and moisture carryover confer ecosystem resilience to moisture stress, the areas we identified where S_{max} commonly exceeds precipitation totals experienced disproportionately high rates of mortality during recent drought. In contrast, the 51-58% of California's total biomass that experiences

15   annually reliable dry-season moisture supply showed lower drought-related mortality. This framework then allows us to use climate projections for the next century to determine that a transition from stable to unstable moisture supply is projected for 3% of the state's carbon stocks. Much of the area presently showing signs of vulnerability is expected to experience additional moisture stress in the coming century due to changes in precipitation amounts alone. An understanding of belowground

20   conditions, including the deep root-zone in bedrock, contributes to prediction of conditions leading to ecosystem water stress.

1 Introduction

Few regions are as vulnerable to projected drought increases as Mediterranean-type seasonally dry ecosystems (Klausmeyer and Shaw, 2009), where peak atmospheric water demand on vegetation coincides with the annually recurring dry season. This amplifies the importance of root-zone water storage (RWS) in determining plant water stress (Klos et al., 2018; Goulden and Bales, 2019; Hahm et al., 2019a). Globally, areas experiencing asynchronicity in water and energy availability host some of the world's major biodiversity hotspots (Underwood et al., 2009), and are projected to significantly expand in their geographic extent under future climate (Feng et al., 2019). Predicting the associated changes in biomass storage and water fluxes will require an understanding of belowground moisture storage dynamics. In Mediterranean settings like California, where energy and water supply are asynchronous, the two major limitations to moisture supply for dry season evapotranspiration (ET_{dry}) are thought to be: (1) the RWS capacity (here termed S_{max}) available to retain water for use in the dry season and (2) the amount of wet season precipitation that enters RWS (Fellows and Goulden, 2017). Hahm et al. (2019a) term these conditions capacity-limited and precipitation-limited storage, respectively.

Capacity-limited places experience stable year-to-year moisture supply at the start of the dry season because net wet season precipitation exceeds S_{max} regardless of annual precipitation amount. In contrast, precipitation-limited places are associated with large swings in moisture availability at the beginning of the dry season that are a function of wet season precipitation. Because S_{max} is not refilled in all years in precipitation-limited places, moisture supply at the onset of the dry season could also depend on precipitation amounts from prior years. Hydrologic memory is a distinct feature of precipitation limitation, because carryover or banking of water supplied in previous years can contribute to ET_{dry} in subsequent years.

Here, we propose to use these classifications as a means of assessing the vulnerability of ecosystems to precipitation shortages. To achieve this, documentation of time-varying RWS and S_{max} is needed. However, RWS is not always well characterized by soil moisture sensing or available datasets on soil water storage capacity. Woody plants commonly access weathered bedrock for moisture in addition to soils, and this behavior is widespread across California (McCormick et al., 2021; Witty et al., 2003; Graham et al., 1997). Geology and bedrock weathering therefore play a strong role in determining root-zone properties such that S_{max} can be highly spatially variable (Hahm et al., 2019b).

Field studies that have documented RWS over time provide evidence for both capacity-limited storage (Hahm et al., 2019b, 2020; Rempe and Dietrich, 2018) and precipitation-limited storage conditions (Goulden and Bales, 2019; Hahm et al., 2022b; Callahan et al., 2022) and reveal contrasting responses of these two categories to drought. Figure 1 illustrates three sites where RWS was directly measured via borehole networks and repeat geophysical logging over multiple years with highly variable precipitation conditions. S_{max} can then be approximated as the largest RWS over the long-term record. At two sites (ACRR and SRR), RWS is roughly the same year-to-year and S_{max} (shown as a red line) is lower than the minimum P_{wy}. At a third site (RV), P_{wy} is often insufficient to replenish storage (Figure 1I). Hahm et al. (2022b) found that in years where P_{wy} fell bellow S_{max}, plants experienced water stress. Precipitation-limited conditions were also observed in intensive study sites in the southern Sierra Nevada, where deep weathering leads to a large S_{max} (Klos et al., 2018) and the multi-year 2012-2016 drought led to mortality (Goulden and Bales, 2019). In these watersheds, despite the large S_{max} that allowed for carryover

storage (Cui et al., 2022), forests were not resilient to multi-year drought (Rungee et al., 2019). It was proposed that progressive drying of RWS in the deep root-zone occurred over multiple drought years following years of canopy expansion (also known as structural overshoot) during wet years prior to the drought (Jump et al., 2017; Goulden and Bales, 2019; Callahan et al., 2022). In contrast, in the western northern California Coast Range, measurements from ACRR and SRR revealed that RWS was

60 replenished annually throughout the 2012-2016 drought despite receiving less than half the mean annual precipitation (Hahm et al., 2019b; Rempe and Dietrich, 2018). These Coast Range forests did not experience significant drought stress or mortality despite the reduction in precipitation, and this is attributed to a small S_{max} relative to P_{wy} (Rempe and Dietrich, 2018).

Building on these field observations, Hahm et al. (2019a) introduced a stochastic hydrologic model for categorizing watersheds into precipitation- and capacity-limited conditions and analyzed 26 watersheds across California, demonstrating that

65 precipitation-limited watersheds experienced drought stress in the 2012-2016 drought, while capacity-limited sites did not. These prior analyses of belowground water storage dynamics have been limited to individual hillslope-scale study sites or watersheds where year-to-year RWS could be estimated via watershed mass balance. In parallel, ecological studies on forest drought response emphasize the importance of hydroclimate and RWS as a driver of ecological response (Keen et al., 2022; Stovall et al., 2019; Yang et al., 2021; Restaino et al., 2019). Thus, RWS serves as a critical missing link between climate,

70 hydrologic mass balance and ecological response.

Here, we harness recent advances in the estimation of RWS via deficit tracking methods (e.g. Wang-Erlandsson et al. (2016); Dralle et al. (2020a); McCormick et al. (2021); Stocker et al. (2023); Lapides et al. (2022)) to investigate the relationship between RWS and precipitation variability across all of California's forest and savanna ecosystems. We introduce three methods for categorizing woody ecosystems as precipitation limited or capacity limited using historical distributed hydroclimate

75 datasets. We then use projected hydroclimate data and our estimates of S_{max} within this framework to predict how forest water stress will be distributed across California over the coming century. By identifying locations that are currently precipitation-limited, and those which may experience precipitation-limited conditions in the future, we provide a prediction of future drought stress or mortality risk.

2   Methods

80 We employ a framework that leverages three distinct water balance methods (described below and illustrated in Figure 2) to classify root-zone water storage (RWS) into two categories: capacity-limited and precipitation-limited, where precipitation-limited conditions are associated with vulnerability to precipitation variability. We limit our analysis to forest and savanna across California at the 500 m pixel scale using the MODIS Land Cover Type dataset (Friedl and Sulla-Menashe, 2015) from 2020 according to the Land Cover Type 1: Annual International Geosphere-Biosphere Programme (IGBP) classification band.

85 We define pixels with woody vegetation as landcover types evergreen needleleaf forests, evergreen broadleaf forests, deciduous broadleaf forests, mixed forests, woody savannas, and savannas. Biomass data is sourced from the 2010 above-ground carbon estimates from (Spawn and Gibbs, 2020), elevation from the NASA Shuttle Radar Topography Mission, SRTM (Farr et al.,

2007), and forest mortality from the U.S. Forest Service Forest Health Aerial Monitoring Program, which we sum over the years 2014-2017 (US Forest Service, 2017a, b).

2.1   Quantification of root-zone water storage capacity

To quantify RWS, we first calculate a time-varying root-zone water storage deficit ($D(t)$) following McCormick et al. (2021) and Dralle et al. (2020a), which build upon Wang-Erlandsson et al. (2016) and others. The deficit quantifies the amount of water used for ET that cannot be explained by contemporaneous precipitation and therefore must result in a net drawdown of subsurface water storage. An example deficit time series is shown in Figure S1. We note that the deficit calculation can be done with any ET or P data sources, including improved remotely sensed data sources as they become available. Here, we emphasize the proposed framework and use publically available spatially distributed evapotranspiration (ET) and precipitation (P) datasets: the Penman-Monteith-Leuning (PML) V2 ET dataset at an 8-day frequency and 500 m resolution (Zhang et al., 2019), which we interpolate to daily frequency, and the Parameter-elevation Regressions on Independent Slopes Model (PRISM) (Daly et al., 2015, 2008) precipitation dataset at a daily frequency and approximately 4600 meter resolution. We selected PML V2 because it is a surface energy balance based method that does not require assumptions about subsurface storage such as soil moisture or plant available water in the calculation of ET (Zhang et al., 2019). Among the surface energy balance based models, we selected PML V2 because it performs better than other ET products when benchmarked with water storage data from the GRACE satellite and water budget information from stream gauges (Chao et al., 2021). Further, because uncertainties in both P and ET impact the estimation of RWS, we evaluate water budget closure for seasonally dry, minimally impacted watersheds in the western U.S. where streamflow data are available (Figure S2). The general agreement between annual streamflow (Q) and P less ET, using the PRISM and PML V2 datasets provides support for using these products for deficit calculations.

We designate the maximum observed value of D over some time period as S_{max} (Eq. 1) which places a conservative lower-bound on the true S_{max} (RWS capacity), which could be much larger but not accessed by vegetation in its entirety over the study period. All precipitation (rain and melted snow) is assumed to enter the root-zone. Drainage out of the root-zone need not be quantified in the approach described below, and lateral groundwater or overland flow into the pixel is assumed to be negligible (see discussion in McCormick et al. (2021); Lapides et al. (2022)). We assume that water availability rather than energy availability limits ET in the summer dry season in California and do not exclude any areas on the basis of energy limitation. We exclude locations where the total ET over the period from 2003 to 2020 exceeds total precipitation (see Figure S3). Over 90% of this excluded area is classified as savanna or woody savanna landcover, with the savanna class, defined as tree cover 10-30% and a canopy >2 m height (Friedl and Sulla-Menashe, 2015), accounting for >75% of the excluded area (Figure S3). We hypothesize that the pixels removed from the study where ET exceeds P are due to ET errors associated with bare ground or herbaceous non-woody vegetation cover.

The simple framework we present here relies on a single value of S_{max} to characterize each pixel. S_{max} is influenced by the combination of long-term processes affecting water retention properties (e.g. porosity, clay fraction) and the contemporary ecosystem and its relationship to atmospheric water demand. We need not assume that S_{max} remains static over the time period of observation, just that S_{max} reflects the maximum possible deficit at that pixel. For example, in the case of disturbance such

4

as fire and mortality, the maximum deficit (which would be used to assign S_{max}) would reflect the period of the maximum observed water use, and likely highest biomass, over the time period of observation. Thus, S_{max} would reflect pre-disturbance conditions and could still be used to assess the potential for future vulnerability without explicitly accounting for the lowering of S_{max} associated with disturbance. We therefore retain locations in the analysis that experienced disturbance, such as fire or drought driven mortality. Future work is needed to evaluate how the evolution of biotically controlled storage capacity impacts drought stress.

In California's Mediterranean climate, the deficit is primarily accrued during the dry season, and may or may not "reset" to zero during the wet season. The deficit can therefore depend on the length of the time series analyzed. Here, we calculate S_{max} as the maximum deficit over the entire available time series (Oct. 1, 2003 to Sept. 30, 2020).

$$S_{max} \equiv max(D(t)), 2003 < t < 2020 \tag{1}$$

We also consider individual water year deficit time series, D_{wy} (Equation 2, dashed line Figure 2B, E), by subdividing the D time-series into water years and resetting the deficit to 0 at the start of each water year.

$$D_{wy}(t) = D(t) Oct1, (wy-1) < t < Sept30, wy; D(Oct1, (wy-1)) = 0 \tag{2}$$

where wy is water year. Limited data are available for validation of a deficit time series or estimates of S_{max}. McCormick et al. (2021) show good agreement between S_{max} used in this study to published values of direct measurements of subsurface storage from individual field sites, however, there are few measurements of year-to-year variations in deficit (including both soil and rock moisture). The only quantitative, field-based deficit measurements of which we are aware come from the three extensively monitored sites in Northern California shown in Figure 1. These sites differ in their combination of geology, vegetation, and precipitation variability. Deficit measurements are made via successive neutron probe logging in deep boreholes that extend beneath the root zone to capture the full depth of dynamic water storage. Differences in neutron count over time are used to arrive at depth integrated measurements of change in water storage (e.g.Rempe and Dietrich (2018)). S_{max} is taken as the largest depth-integrated deficit measured with the neutron probe. In-situ measurements of S_{max} averaged across boreholes correspond to remotely sensed estimates (Table S1). However, the field based measurements are inherently limited in their spatial coverage relative to the 500 m pixel size we use to calculate deficits. Upscaling approaches and additional measurements are thus needed to validate deficit time series using remote sensing data.

Method 1: Correlation between water year precipitation and dry season evapotranspiration

Method 1 is based on Hahm et al. (2019a), which categorizes storage into precipitation limited and capacity limited based on the Spearman rank correlation between P_{wy} and a watershed mass-balance estimated storage on April 1. Here, we classify pixels as either precipitation-limited or capacity-limited using the Spearman rank correlation between water year precipitation (P_{wy}) and dry season ET (ET_{dry}), under the assumption that ET_{dry} scales with RWS at the end of the wet season. A high

correlation coefficient between P_{wy} and ET_{dry} (ρ approaching 1) is consistent with precipitation limitation (i.e. sensitivity of ET_{dry} to interannual variability in precipitation) and low correlation (ρ approaching 0) indicates insensitivity of ET_{dry} to precipitation consistent with capacity limitation. To define the threshold between capacity and precipitation limitation, we used the median value of ρ (0.35) across the dataset.

Method 2: Identification of carryover storage

The objective of Method 2 is to identify locations where variability in storage year to year occurs because insufficient wet season precipitation arrives to fill deficits accrued during the preceding dry season. If the running deficit is not reset by P_{wy}, then, by mass balance, ET_{dry} must be derived from storage that arrived in a previous wet season, which we term carryover storage. We note that the water sourced by plants in any given year could have a wide age distribution, which includes water from a previous year (Hahm et al., 2022a), however, we focus on the conditions where, by mass balance, ET_{dry} must be derived from carryover. Use of carryover storage is representative of precipitation limitation because it reflects year-to-year differences in RWS at the start of the dry season. Capacity-limited conditions are instead associated with low to no year-to-year variability in RWS entering the dry season.

To quantify carryover storage, we calculate the difference between S_{max} and the maximum deficit that can be accrued in a single water year at the site ($max(D_{wy})$). We report this value as a percentage of S_{max} and term it the fractional carryover storage, C. Note that carryover storage is dependent on the existence of a large enough drought during the study period to result in multi-year storage draw-down.

$$C = \frac{1}{S_{max}} * (S_{max} - max(D_{wy})) \tag{3}$$

Pixels are classified as precipitation limited if C is greater than 10% of S_{max} (Eq. 3).

Method 3: Comparison of annual precipitation distribution to RWS capacity, S_{max}

We classify capacity-limited conditions as pixels where net precipitation (approximated by P_{wy}) always exceeds S_{max}. Precipitation limitation, in contrast, is classified here by at least one observed value of P_{wy} falling below S_{max}, implying that storage would not be refilled in a year when P_{wy} is less than S_{max}. A percentile rank of S_{max} relative to the historical P_{wy} greater than 0% is used to classify pixels as precipitation limited. We use the distribution of P_{wy} from 1980 to 2020. This method is based on the proposal by Hahm et al. (2019a) that the relationship between S_{max} and the statistical distribution of net precipitation is a good predictor of ET_{dry} and water stress.

To assess how woody vegetation may respond to future precipitation conditions, we compare the projected distribution of precipitation to S_{max}. We make the assumption that S_{max} remains the same, but the distribution of P_{wy} is represented by projections of annual precipitation from 2060 to 2100 from 10 downscaled Global Climate Models (GCMs) (Persad et al., 2020; Pierce et al., 2014, 2018). The 10 models were chosen by the California Climate Change Technical Advisory Group (CCTAG, 2015) as best representing the historical behavior of California-specific climate and hydrological parameters among

all contemporaneous GCMs. Details on the specific GCMs, the downscaling method, and the extraction of annual precipitation can be found in (Persad et al., 2020; Pierce et al., 2014, 2018). We use the same number of years as the historical analysis (n=40) and the most temporally distant available years in order to separate the past and future scenarios to allow time for the divergence of the climate regime. We use the RCP 4.5, Representative Concentration Pathway 4.5 future emissions scenario (Meinshausen et al., 2011; Thomson et al., 2011)), which was developed for the Fifth Assessment Report of the Intergovernmental Panel on Climate Change (IPCC AR5) as a "medium stabilization" scenario.

3 Results

The three proposed methods are applied across California to classify woody ecosystems as exhibiting precipitation-limited storage or capacity-limited storage behavior (Figure 2). Two example sites illustrate the three methods. At the capacity-limited location, shown as the top panel in Figure 2a-c, ET_{dry} is consistent year-to-year and poorly correlated with P_{wy} (Method 1, Figure 2a; Spearman ρ = -0.18). The RWS deficit time series shown in Figure 2b shows that deficits that are accrued in the dry season are reset every wet season and reach approximately the same maximum value every year (Method 2, fractional carryover storage (C) = 0). Finally, historical values of P_{wy} reliably exceed S_{max} (Method 3, Figure 2c; probability of $P_{wy} < S_{max}$ = 0). Even during drought years (2012-2016), precipitation is sufficient to reset deficits to zero each wet season, indicating that carryover storage is not needed to explain ET. At the precipitation-limited location shown in Figure 2d-f, wetter years are associated with more ET_{dry} (Method 1, Figure 2d; Spearman ρ = 0.76). The deficit may not reset to zero during the wet season and can even accrue over multiple years, indicating use of carryover storage (Method 2, Figure 2e). At this site, carryover storage can account for up to 49% of S_{max}, indicating that some ET_{dry} in a given year is sourced from precipitation delivered in previous years. Finally, the probability that P_{wy} will be less than S_{max} is 63% (Method 3, Figure 2f). At this location, there was tree mortality associated with the 2012-2015 drought (US Forest Service, 2017a).

Annual variability in root-zone water storage

Precipitation-limited and capacity-limited locations are mapped across California in Figure 2G-I following the three methods illustrated in Figure 2A-F. Gray areas are classified as capacity limited and colors reflect the degree of precipitation limitation. There is general agreement in the spatial distribution of the two limitation categories across all three approaches (Figure S4), though areas with the lowest mean annual precipitation show the strongest agreement (Figure S5). Methods 1-3 categorize 28, 29, and 33% (35,740 - 42,320 km^2) of the area hosting woody ecosystems as precipitation limited, representing 16, 19, and 23% of California aboveground carbon stocks.

Our classification of ACRR and SRR as capacity-limited and RV as precipitation-limited using the methods proposed here is consistent with the RWS dynamics observed at each site (Rempe and Dietrich, 2018; Hahm et al., 2019b, 2022b). RWS quantified via repeat neutron probe surveys in boreholes over multiple years revealed refilling of storage to S_{max} annually at ACRR (Rempe and Dietrich, 2018; Hahm et al., 2019b). In contrast, storage at the RV site in the deeply weathered Great Valley Sequence (GVs) is precipitation limited, with RWS monitoring data revealing carryover of moisture from one year to

7

215 the next and incomplete refilling of RWS during dry years (Pedrazas et al., 2021; Hahm et al., 2022b). Notably, ACRR and SRR, which are located across a geologic fault, experience similar distributions of P_{wy} and are both classified as capacity limited, yet their vegetation composition and total above-ground biomass differ, which reflects the differences in the magnitude of S_{max}. Agreement between precipitation measured at each site and PRISM lends support to deficit calculations made with PRISM precipitation (Figure S6). Our assessment of S_{max} and assignment of precipitation- and capacity-limited storage at the

220 pixel scale shows general agreement with watershed based assessments by previous investigators including Sequoia groves in the Sierra (Cui et al., 2022) and 26 watersheds across California (Hahm et al., 2019a).

Across California, savannas tend to be precipitation-limited relative to forests: of the total forest area, only 10, 17, and 25% is precipitation limited (5,000, 87,000, and 12,700 km^2, Methods 1-3), while 36, 38, 40% of total savanna area is precipitation limited (28,300, 29,600, and 30,600 km^2, Methods 1-3). Indeed, areas with more aboveground biomass tend to be more

225 capacity limited (Figure 3a). Extremely wet and extremely dry areas tend to be associated with capacity and precipitation limitation, respectively (Figure 3b). Nearly all locations with mean annual precipitation (MAP) greater than 1250 mm/year are capacity limited and nearly all locations with MAP less than 500 mm/year are precipitation limited (Figure 3b). However, the majority California's woody vegetation occurs at intermediate MAP (500-1250 mm), where both precipitation and capacity limitation occur and there is some disagreement across the three methods (Figure S4). High elevation areas (>2500 km) tend to

230 be capacity limited; however, precipitation limitation is seen to a similar degree for all other elevations (Figure 3c). Capacity-limited behavior in high elevation or high MAP areas may reflect other limitations to ET_{dry} such as energy limitation.

Tree mortality (summed over the years 2014 to 2017) is associated with locations characterized as precipitation limited (Figure 3d). To test if the association between precipitation limitation and mortality results from using deficits calculated during the extreme 2012-2016 drought, we analyzed a shorter time series ending in 2012 and found that this association was

235 maintained across all three methods, whereby the likelihood of precipitation limitation (by area) is higher for places that experienced high mortality (Figure S7). We therefore conclude that mortality is likey associated with precipitation limitation.

Projected shifts in root-zone water supply

Precipitation-limited areas that are projected to experience an increase in the number of years where P_{wy} falls below S_{max} are shown in Figure 4, where the color represents the number of global climate models that agree on this shift (see Methods).

240 These areas could be considered the most vulnerable and likely to see increases in water stress. The 11,950 km^2 area where 5 or more models agree on this shift host approximately 5% of the above-ground carbon stocks in the state (55 Tg of carbon). For capacity-limited areas, which do not presently experience years with P_{wy} below S_{max}, we identify where projections indicate precipitation reduction below S_{max} (orange areas in Figure 4). The transition from capacity limitation to precipitation limitation is expected to increase water stress. The 5,160 km^2 area where 5 or more models agree on this shift host approximately 3% of

245 the carbon stocks in the state (27 Tg of carbon). Together, considering both potential shifts, a total of 8% of the biomass (82 Tg of carbon) - representing 16% of the forest and savanna area in the state - is expected to experience increased water stress over the next century due to changes in the relationship between RWS and precipitation. Substantial fractions of protected national parks and forests are projected to experience an increase in water stress or a potential transition from capacity to precipitation

limitation (Figure 4), including almost the entirety of the Sierra National Forest and Los Padres National Forest. Conversely, the majority of the northern California Coast Ranges and high elevation areas of the northern Sierra Nevada are not projected to transition from capacity to precipitation limitation conditions based on shifts in precipitation alone. In these areas, a >40% reduction in P_{wy} during the driest years (the lowest 25th percentile of P_{wy}) would be needed to create a condition where S_{max} is not replenished (Figure S8). These locations are the least vulnerable to changing RWS in our analysis. However, we do not account for amplified warming or decreased snow fraction, which are projected across high elevation regions and will increase reliance on RWS.

4 Discussion & Conclusion

By quantifying time varying RWS and its relationship to S_{max} and P_{wy}, we map where forests and savannas have increased likelihood of experiencing water stress due to interannual variations in annual precipitation (Figure 2G-I, colored areas). The proposed framework answers the call from plant ecophysiology studies for better incorporation of the subsurface to understand distributions of mortality (Dawson et al., 2020) and provides context for assessment of wildfire vulnerability (Rao et al., 2022) and carbon storage for nature-based climate solutions (Coffield et al., 2021; Tague and Moritz, 2019). While proximate causes of mortality can be complex, water stress is considered a central prerequisite (Trugman et al., 2021; Anderegg et al., 2012). Our finding that high mortality areas are more commonly precipitation limited suggests that the methods presented here could be used to quantify mortality risk. Of the three methods, Method 1 showed the lowest likelihood of precipitation limitation for areas experiencing substantial mortality. This suggests that use of carryover storage (detected by Method 2) and low S_{max} relative to P_{wy} (Method 3) may be useful indicators of mortality risk due to water stress.

To compare vulnerability across different locations, in addition to assuming that data uncertainty is spatially uniform, we must also assume that all locations experienced drought conditions severe enough to deplete the root-zone water storage capacity (S_{max}) over the time period of observation (2003-2020). While nearly the entire state of California experienced "exceptional drought" between 2014 and 2016 (National Drought Mitigation Center et al., 2019), there may be locations where the S_{max} calculated here is underestimated because sufficiently severe drought conditions did not occur between 2003 and 2020. New methods have been proposed recently to assess the S_{max} outside of the range of deficits achieved during a period of observation (Stocker et al., 2023; Dralle et al., 2020b). These methods could be applied in the future to evaluate locations where S_{max} may be underestimated.

We also report where woody ecosystems have large enough S_{max} to bank precipitation for multiple years via carryover storage (Figure 2H). In this case, large S_{max} may confer drought resilience in the sense that plants can sustain transpiration through years of drought, but it may also lead to the build-up of large root-zone storage deficits that cannot be quickly replenished, resulting in vulnerability, not resilience, to precipitation reductions in larger droughts (Goulden and Bales, 2019; Hahm et al., 2022b). Carryover storage may also be the hydrological manifestation of structural overshoot by the plant community, wherein high biomass density generates storage deficits that cannot be replenished during dry years. The widespread use of carryover storage suggests that plant communities may experience other forms of limitation than water stress in the long, dry California

9

summer, because not all water that is plant available is used in a given year. Open questions remain about the mechanisms by which water volumes unused in a previous dry season are accessed in the following year; however recent work suggests that the mechanism may be related to new root growth. For example, increased investment in belowground biomass to mine decades-old water has been reported (Zhang et al., 2017).

In both capacity-limited and precipitation-limited areas, S_{max} commonly exceeds reported values of soil water storage capacity (Figure S9). This additional root-zone water supply is likely sourced from the underlying weathered bedrock as either rock moisture or groundwater, with the former likely being more common in California (McCormick et al., 2021). Here, we exclude areas where ET exceeds P over the long term indicating a stable water source to vegetation that is decoupled from rainfall, such as lateral groundwater contribution (see Materials and Methods). Such conditions, while also potentially vulnerable to projected climate change (McLaughlin et al., 2017), are not considered here. Incorporating deeper plant-available water storage in weathered bedrock in ecohydrologic models can improve estimation of evapotranspiration under drought conditions (Fowler et al., 2021). Weathered bedrock water storage dynamics are beginning to be incorporated into ecohydrologic models (La Follette et al., 2022; Jiménez-Rodríguez et al., 2022) with the results presented here serving as an important constraint to such models. The geologic controls on S_{max} remain an open question, as highlighted by the large variability in S_{max} over regions receiving high precipitation (Figure S5).

There are several widely used metrics for assessing drought stress, such as Climatic Water Deficit (CWD) and the Palmer Drought Severity Index (PDSI). The framework proposed here relies on the relationship between root-zone water storage deficit and S_{max} (i.e. the maximum observed deficit over a period of record.) This relationship serves as a relative metric of water stress in that it provides a quantitative means of assessing how much infiltration is needed to return to non-drought conditions. Unlike PDSI and CWD, the root-zone water storage deficit and S_{max} are measurable quantities in a landscape (e.g. Hahm et al. (2022b)) and can be used to predict water stress before evapotranspiration is water limited. For example, in the instance of year over year deficit accrual (i.e. carryover), such as during the 2014-2016 drought in the southern Sierra Nevada, the high ET sustained through drought conditions may have led to a relatively low CWD. The continual depletion of storage - indicative of future water stress - was reflected in the deficit as a fraction of S_{max}. We propose that better estimates of root-zone water storage deficit and its relationship to S_{max} will contribute to existing drought predictors.

Annual precipitation projections for California and other Mediterranean regions show a wide range of outcomes, not only between GCMs but also among different future emission trajectories (Persad et al., 2020). Yet our results indicate that widespread water stress increases are expected for the projected precipitation changes even in the face of this GCM range and using a relatively optimistic climate change scenario (see Methods). Factors in addition to rainfall shortages - such as the projected increase in temperatures and vapor pressure deficit (Bedsworth et al., 2018; Luo et al., 2017) and changes in plant water use efficiency - are likely to impact future water stress. Additionally, decreases in spring precipitation increasing instances of multi-year drought, low to no snow years, and alternation between extreme wet and dry years (Persad et al., 2020; Swain et al., 2018; Harsch et al., 2009) are all projected for California. All of these conditions are likely to lead to greater water stress attributable to longer dry periods, lower net precipitation, or increases in atmospheric demand. By accounting for the impact of rainfall

variability on root-zone water supply, our results provide a belowground constraint that can contribute to the determination of future water stress (Asner et al., 2016; Anderegg et al., 2018; Konings et al., 2021).

Beyond plant vulnerability to drought, the use of carryover storage and multi-year deficit accrual associated with precipitation limitation has been linked to declines in runoff following drought (Lapides et al., 2022), suggesting that watersheds with precipitation-limited areas shown in Figure 2G-I may be prone to greater hydrologic memory of drought. Understanding the relationship between RWS and precipitation variability may be key to identifying the conditions by which plant community shifts or changes to atmospheric demand impact streamflow. Improved documentation of RWS deficits and precipitation limitation can thus contribute to water resource and forestry decision making.

Figure 1. Three locations where RWS in soils and weathered bedrock has been documented via direct observation are marked as stars. Maps denote the Coastal Belt, Central Belt, and Great Valley Sequence (GVs) geologic boundaries overlaying satellite imagery in Northern California. Bottom left panel shows descriptions and hillslope cross sections for the three study sites: The Angelo Coast Range Reserve (ACRR, also shown in Figure 2A-C), Sagehorn-Russell Ranch (SRR), and Rancho Venada (RV). Locations of boreholes for monitoring RWS are shown as gray lines overlying hillslope cross sections. S_{max} was estimated at each site via long-term neutron probe monitoring of RWS dynamics and reported in Rempe and Dietrich (2018) (ACRR), Hahm et al. (2020) (SRR) and Hahm et al. (2022b) (RV). S_{max} is shown as red vertical lines on histograms of wateryear precipitation (P_{wy}) from 1980-2021 for each site (Daly et al., 2008). The width of the red line indicates the maximum measured range of S_{max} across the borehole network due to variability in e.g. root-zone depth, hillslope aspect, and hillslope position. RWS includes storage in soils at all sites, however bedrock water storage (i.e. rock moisture) dominates storage capacity at these sites (McCormick et al., 2021; Rempe and Dietrich, 2018; Hahm et al., 2020, 2022b). ACRR and SRR exhibit capacity-limited behavior, because P_{wy} consistently exceeds S_{max} - including during dry years - and field measurements reflect low year-to-year RWS temporal variability (Rempe and Dietrich, 2018; Hahm et al., 2020). In contrast, RV exhibits precipitation-limited storage, because in dry years S_{max} exceeds P_{wy} and storage does not refill (Hahm et al., 2022b).
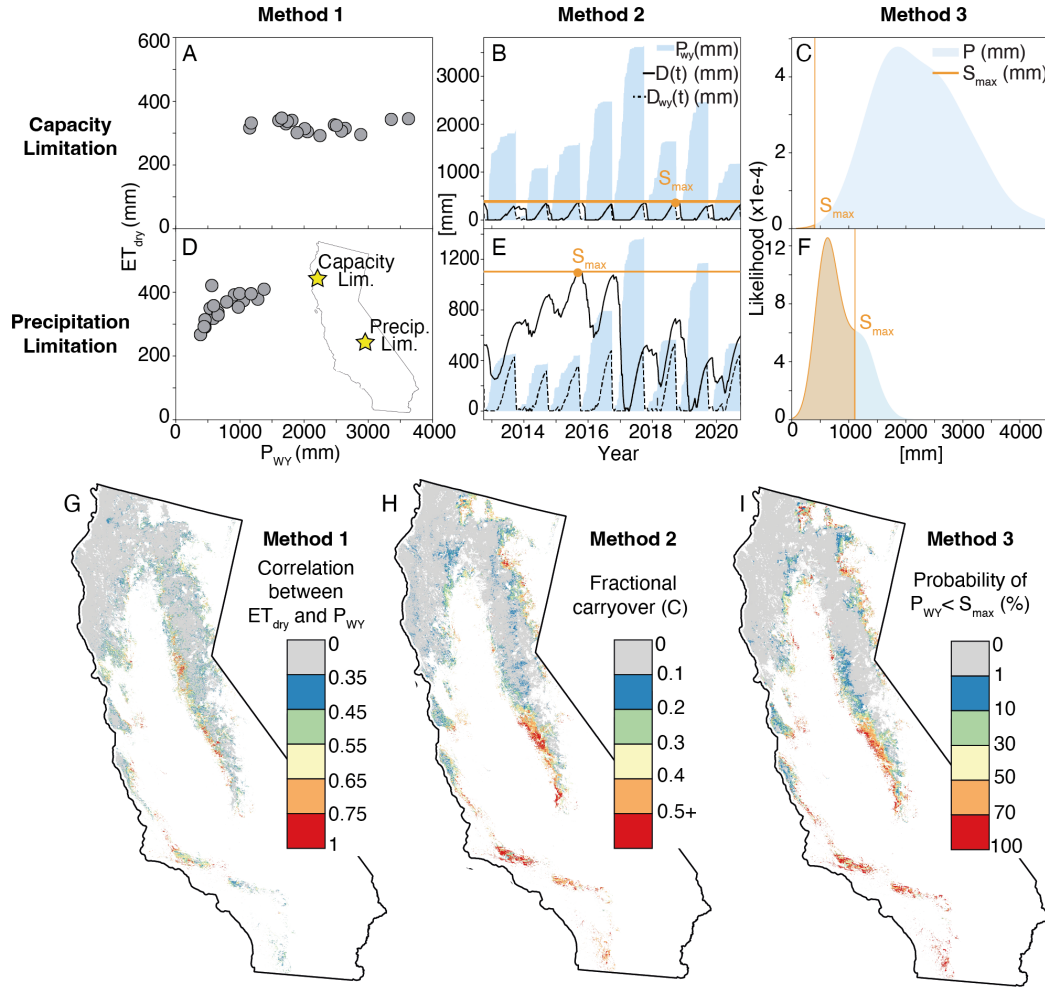
Figure 2. Characterization of capacity-limited and precipitation-limited conditions across two example sites (A-F) and California (G-I). Each vertical panel represents one of three methods employed (see Methods). Examples of a capacity-limited site (A-C) and a precipitation-limited site (D-F) illustrate the three methods. Locations of the two sites are shown in inset in D. From left to right: (A,D) Dry-season ET (ET_{dry}) as a function of water year precipitation (P_{wy}) for water years 2003 to 2020; (B,E) time-series of the total and water year root-zone water storage deficit ($D(t)$ and $D_{wy}(t)$) from 2012 to 2020 (see Materials and Methods). Full time-series from 2003 to 2020 is shown in Figure S1. Precipitation is shown in blue and orange denotes the root-zone water storage capacity (S_{max}), inferred from the largest observed deficit, D(t). The fractional carryover storage (C) is calculated as the difference between S_{max} and max(D_{wy}) and normalized by S_{max}; (C,F) distribution of historical P_{wy} from 1980-2020 with the minimum estimate of S_{max} shown in orange. (G-I) Grey pixels represent capacity-limited woody vegetation as measured by each method, colored areas represent precipitation-limited woody vegetation, and areas in white are not classified as woody vegetation or are places where ET exceeds P over the study period (Figure S2). Agreement between three methods is shown in Figure S4 and S_{max} is shown in Figure S10. P-values for correlations correspond well to ρ indicating a significant correlation between P_{wy} and ET_{dry} (p-value ≤ 0.05) in precipitation-limited locations (Figure S11).
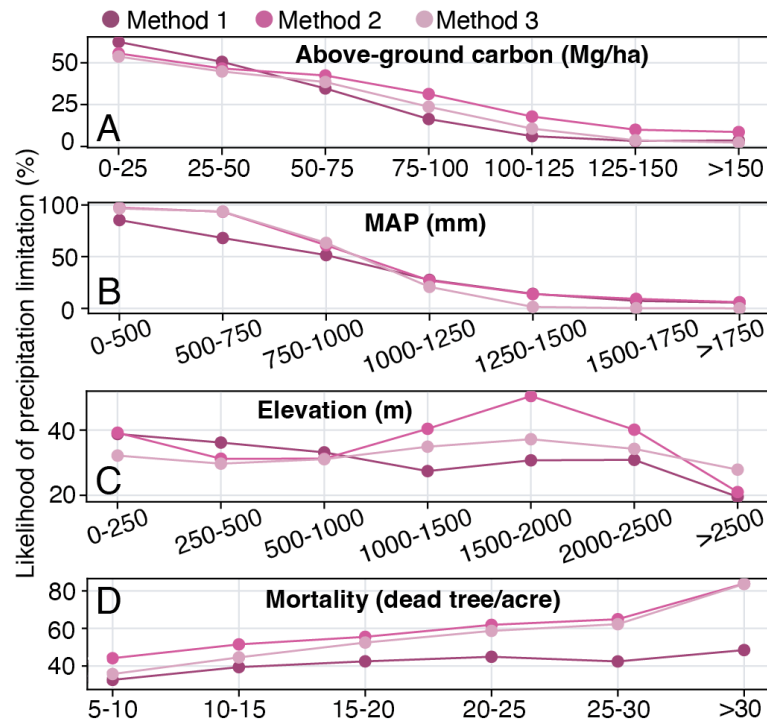
Figure 3. The likelihood of precipitation limitation across California's woody plant communities as a function of (A) above-ground carbon, (B) mean annual precipitation (MAP), (C) elevation, and (D) tree mortality from 2014-2017. Likelihood is defined as the proportion of an area of a particular class (represented as bins on the x-axis) that is categorized as precipitation limited. In Figure S5, the areas of each bin are reported. In Figure S7, these relationships are reported for a deficit time series that ends prior to the major drought that started in 2012. Note variable y-axis limits across subplots.

References

Anderegg, W. R., Berry, J. A., and Field, C. B.: Linking definitions, mechanisms, and modeling of drought-induced tree death, Trends in
335   plant science, 17, 693–700, 2012.

Anderegg, W. R. L., Konings, A. G., Trugman, A. T., Yu, K., Bowling, D. R., Gabbitas, R., Karp, D. S., Pacala, S., Sperry, J. S., Sulman, B. N., and Zenes, N.: Hydraulic diversity of forests regulates ecosystem resilience during drought, Nature, 561, 538–541, https://doi.org/10.1038/s41586-018-0539-7, 2018.

Asner, G. P., Brodrick, P. G., Anderson, C. B., Vaughn, N., Knapp, D. E., and Martin, R. E.: Progressive forest canopy water loss during the
340   2012–2015 California drought, Proceedings of the National Academy of Sciences, 113, https://doi.org/10.1073/pnas.1523397113, 2016.

Bedsworth, L., Cayan, D. R., Franco, G., Fisher, L., Ziaja, S., and Ackerly, D. D.: Statewide Summary Report, California's Fourth Climate Change Assessment, Governor's Office of Planning and Research, 2018.

Callahan, R. P., Riebe, C. S., Sklar, L. S., Pasquet, S., Ferrier, K. L., Hahm, W. J., Taylor, N. J., Grana, D., Flinchum, B. A., Hayes, J. L., et al.: Forest vulnerability to drought controlled by bedrock composition, Nature Geoscience, 15, 714–719, 2022.
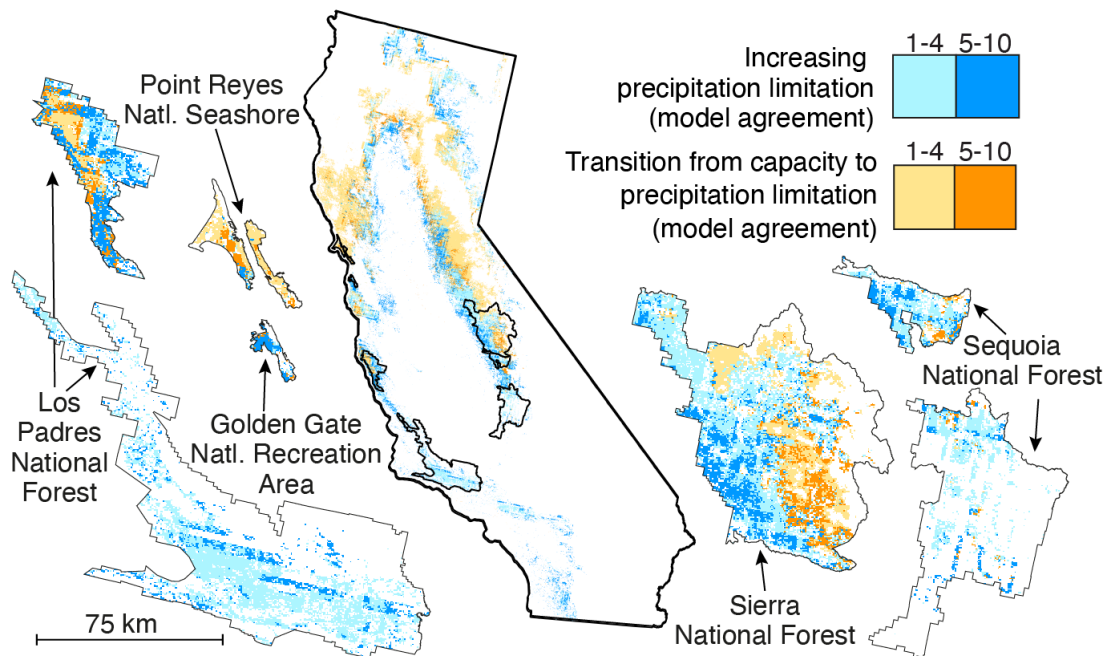
Figure 4. Shifts in root-zone water storage (RWS) reflecting less favorable conditions and increased water stress under precipitation projected for 2060-2100 (see Methods). Ten climate model projections of precipitation variability are used (see Materials and Methods) to identify (in blue) locations presently characterized as precipitation limited where projected decreases in precipitation will lead to a lower probability of annual precipitation meeting or exceeding S_{max} and (in orange) locations where projected decreases in precipitation will result in a transition from capacity-limited to precipitation-limited conditions. Colors reflect the number of models (out of 10) that agree on the change. Pop-outs show model agreement for select national parks and forests. Scale bar refers to pop-outs. We note that S_{max} is at a finer resolution (500 m) than the projected precipitation variability data (downscaled to 1/16th degree longitude by latitude Persad et al. (2020)).

345   CCTAG: Perspectives and Guidance for Climate Change Analysis, 2015.

Chao, L., Zhang, K., Wang, J., Feng, J., and Zhang, M.: A comprehensive evaluation of five evapotranspiration datasets based on ground and grace satellite observations: Implications for improvement of evapotranspiration retrieval algorithm, Remote Sensing, 13, 2414, 2021.

Coffield, S. R., Hemes, K. S., Koven, C. D., Goulden, M. L., and Randerson, J. T.: Climate-driven limits to future carbon storage in California's wildland ecosystems, Agu Advances, 2, e2021AV000 384, 2021.

350   Cui, G., Ma, Q., and Bales, R.: Assessing multi-year-drought vulnerability in dense Mediterranean-climate forests using water-balance-based indicators, Journal of Hydrology, 606, 127 431, https://doi.org/10.1016/j.jhydrol.2022.127431, 2022.

Daly, C., Halbleib, M., Smith, J. I., Gibson, W. P., Doggett, M. K., Taylor, G. H., Curtis, J., and Pasteris, P. P.: Physiographically Sensitive Mapping of Climatological Temperature and Precipitation across the Conterminous United States, International Journal of Climatology, 28, 2031–2064, https://doi.org/10.1002/joc.1688, 2008.

355   Daly, C., Smith, J. I., and Olson, K. V.: Mapping Atmospheric Moisture Climatologies across the Conterminous United States, PLOS ONE, 10, e0141 140, https://doi.org/10.1371/journal.pone.0141140, 2015.

Dawson, T. E., Hahm, W. J., and Crutchfield-Peters, K.: Digging Deeper: What the Critical Zone Perspective Adds to the Study of Plant Ecophysiology, New Phytologist, 226, 666–671, https://doi.org/10.1111/nph.16410, 2020.

Dralle, D. N., Hahm, W. J., Chadwick, K. D., McCormick, E., and Rempe, D. M.: Technical Note: Accounting for Snow in the Estimation of

360   Root-Zonewater Storage Capacity from Precipitation and Evapotranspirationfluxes, Hydrology and Earth System Sciences Discussions, https://doi.org/10.5194/hess-2020-602, 2020a.

Dralle, D. N., Hahm, W. J., Rempe, D. M., Karst, N., Anderegg, L. D. L., Thompson, S. E., Dawson, T. E., and Dietrich, W. E.: Plants as Sensors: Vegetation Response to Rainfall Predicts Root-Zone Water Storage Capacity in Mediterranean-Type Climates, Environmental Research Letters, 15, 104 074, https://doi.org/10.1088/1748-9326/abb10b, 2020b.

365 Farr, T. G., Rosen, P. A., Caro, E., Crippen, R., Duren, R., Hensley, S., Kobrick, M., Paller, M., Rodriguez, E., Roth, L., et al.: The shuttle radar topography mission, Reviews of geophysics, 45, 2007.

Fellows, A. W. and Goulden, M. L.: Mapping and Understanding Dry Season Soil Water Drawdown by California Montane Vegetation, Ecohydrology, 10, e1772, http://onlinelibrary.wiley.com/doi/abs/10.1002/eco.1772, 2017.

Feng, X., Thompson, S. E., Woods, R., and Porporato, A.: Quantifying asynchronicity of precipitation and potential evapotranspiration in

370   Mediterranean climates, Geophysical Research Letters, 46, 14 692–14 701, 2019.

Fowler, K. J., Coxon, G., Freer, J. E., Knoben, W. J., Peel, M. C., Wagener, T., Western, A. W., Woods, R. A., and Zhang, L.: Towards more realistic runoff projections by removing limits on simulated soil moisture deficit, Journal of Hydrology, 600, 126 505, 2021.

Friedl, M. and Sulla-Menashe, D.: MCD12Q1 MODIS/Terra+ aqua land cover type yearly L3 global 500m SIN grid V006 [data set], NASA EOSDIS Land Processes DAAC, 10, 2015.

375 Goulden, M. L. and Bales, R. C.: California forest die-off linked to multi-year deep soil drying in 2012–2015 drought, Nature Geoscience, 12, 632–637, https://doi.org/10.1038/s41561-019-0388-5, 2019.

Graham, R. C., Sternberg, P. D., and Tice, K.R.: Morphology, Porosity, and Hydraulic Conductivity of Weathered Granitic Bedrock and Overlying Soils, Soil Science Society of America Journal, 61, 516–522, https://doi.org/10.2136/sssaj1997.03615995006100020021x, 1997.

Hahm, W., Lapides, D., Rempe, D., McCormick, E., and Dralle, D.: The Age of Evapotranspiration: Lower-Bound Constraints From Dis-

380   tributed Water Fluxes Across the Continental United States, Water Resources Research, 58, e2022WR032 961, 2022a.

Hahm, W. J., Dralle, D. N., Rempe, D. M., Bryk, A. B., Thompson, S. E., Dawson, T. E., and Dietrich, W. E.: Low Subsurface Water Storage Capacity Relative to Annual Rainfall Decouples Mediterranean Plant Productivity and Water Use From Rainfall Variability, Geophysical Research Letters, 46, 6544–6553, https://doi.org/10.1029/2019gl083294, 2019a.

Hahm, W. J., Rempe, D. M., Dralle, D. N., Dawson, T. E., Lovill, S. M., Bryk, A. B., Bish, D. L., Schieber, J., and Dietrich, W. E.: Litholog-

385   ically Controlled Subsurface Critical Zone Thickness and Water Storage Capacity Determine Regional Plant Community Composition, Water Resources Research, 55, 3028–3055, https://doi.org/10.1029/2018wr023760, 2019b.

Hahm, W. J., Rempe, D. M., Dralle, D. N., Dawson, T. E., and Dietrich, W. E.: Oak Transpiration Drawn From the Weathered Bedrock Vadose Zone in the Summer Dry Season, Water Resources Research, 56, https://doi.org/10.1029/2020wr027419, 2020.

Hahm, W. J., Dralle, D. N., Sanders, M., Bryk, A. B., Fauria, K. E., Huang, M.-H., Hudson-Rasmussen, B., Nelson, M. D., Pedrazas, M. A.,

390   Schmidt, L. M., et al.: Bedrock vadose zone storage dynamics under extreme drought: consequences for plant water availability, recharge, and runoff, Water Resources Research, https://doi.org/10.1029/2021WR031781, 2022b.

Harsch, M. A., Hulme, P. E., McGlone, M. S., and Duncan, R. P.: Are treelines advancing? A global meta-analysis of treeline response to climate warming, Ecology letters, 12, 1040–1049, 2009.

Jiménez-Rodríguez, C. D., Sulis, M., and Schymanski, S.: Exploring the role of bedrock representation on plant transpiration response during

395   dry periods at four forested sites in Europe, Biogeosciences Discussions, pp. 1–37, 2022.

Jump, A. S., Ruiz-Benito, P., Greenwood, S., Allen, C. D., Kitzberger, T., Fensham, R., Martínez-Vilalta, J., and Lloret, F.: Structural overshoot of tree growth with climate variability and the global spectrum of drought-induced forest dieback, Global change biology, 23, 3742–3757, 2017.

Keen, R. M., Voelker, S. L., Wang, S.-Y. S., Bentz, B. J., Goulden, M. L., Dangerfield, C. R., Reed, C. C., Hood, S. M., Csank, A. Z., Dawson,

400   T. E., et al.: Changes in tree drought sensitivity provided early warning signals to the California drought and forest mortality event, Global Change Biology, 28, 1119–1132, 2022.

Klausmeyer, K. R. and Shaw, M. R.: Climate change, habitat loss, protected areas and the climate adaptation potential of species in Mediterranean ecosystems worldwide, PloS one, 4, e6392, 2009.

Klos, P. Z., Goulden, M. L., Riebe, C. S., Tague, C. L., O'Geen, A. T., Flinchum, B. A., Safeeq, M., Conklin, M. H., Hart, S. C., Berhe, A. A.,

405   Hartsough, P. C., Holbrook, W. S., and Bales, R. C.: Subsurface Plant-Accessible Water in Mountain Ecosystems with a Mediterranean Climate, WIREs Water, 5, e1277, https://doi.org/10/gfdb86, 2018.

Konings, A. G., Saatchi, S. S., Frankenberg, C., Keller, M., Leshyk, V., Anderegg, W. R. L., Humphrey, V., Matheny, A. M., Trugman, A., Sack, L., Agee, E., Barnes, M. L., Binks, O., Cawse-Nicholson, K., Christoffersen, B. O., Entekhabi, D., Gentine, P., Holtzman, N. M., Katul, G. G., Liu, Y., Longo, M., Martinez-Vilalta, J., McDowell, N., Meir, P., Mencuccini, M., Mrad, A., Novick, K. A.,

410   Oliveira, R. S., Siqueira, P., Steele-Dunne, S. C., Thompson, D. R., Wang, Y., Wehr, R., Wood, J. D., Xu, X., and Zuidema, P. A.: Detecting forest response to droughts with global observations of vegetation water content, Global Change Biology, 27, 6005–6024, https://doi.org/10.1111/gcb.15872, _eprint: https://onlinelibrary.wiley.com/doi/pdf/10.1111/gcb.15872, 2021.

La Follette, P. T., Hahm, W. J., Rempe, D. M., Dietrich, W. E., Brauer, C. C., Weerts, A. H., and Dralle, D. N.: Multicriteria analysis on rock moisture and streamflow in a rainfall-runoff model improves accuracy of model results, Hydrological Processes, p. e14536, 2022.

415   Lapides, D. A., Hahm, W. J., Rempe, D. M., and Dralle, D. N.: Missing snowmelt runoff following drought explained by root-zone storage deficits, Pre-print, https://doi.org/10.31223/X5591F, 2022.

Luo, L., Apps, D., Arcand, S., Xu, H., Pan, M., and Hoerling, M.: Contribution of temperature and precipitation anomalies to the California drought during 2012–2015, Geophysical Research Letters, 44, 3184–3192, 2017.

McCormick, E. L., Dralle, D. N., Hahm, W. J., Tune, A. K., Schmidt, L. M., Chadwick, K. D., and Rempe, D. M.: Widespread woody plant

420   use of water stored in bedrock, Nature, 597, 225–229, 2021.

McLaughlin, B. C., Ackerly, D. D., Klos, P. Z., Natali, J., Dawson, T. E., and Thompson, S. E.: Hydrologic refugia, plants, and climate change, Global change biology, 23, 2941–2961, 2017.

Meinshausen, M., Smith, S. J., Calvin, K., Daniel, J. S., Kainuma, M. L., Lamarque, J.-F., Matsumoto, K., Montzka, S. A., Raper, S. C., Riahi, K., et al.: The RCP greenhouse gas concentrations and their extensions from 1765 to 2300, Climatic change, 109, 213–241, 2011.

425   National Drought Mitigation Center, US Department of Agriculture, and National Oceanic and Atmospheric Administration: United States Drought Monitor, https://data.nal.usda.gov/dataset/united-states-drought-monitor, 2019.

Pedrazas, M. A., Hahm, W. J., Huang, M.-H., Dralle, D., Nelson, M. D., Breunig, R. E., Fauria, K. E., Bryk, A. B., Dietrich, W. E., and Rempe, D. M.: The relationship between topography, bedrock weathering, and water storage across a sequence of ridges and valleys, Journal of Geophysical Research: Earth Surface, 126, e2020JF005 848, 2021.

430   Persad, G. G., Swain, D. L., Kouba, C., and Ortiz-Partida, J. P.: Inter-Model Agreement on Projected Shifts in California Hydroclimate Characteristics Critical to Water Management, Climatic Change, 162, 1493–1513, https://doi.org/10.1007/s10584-020-02882-4, 2020.

Pierce, D. W., Cayan, D. R., and Thrasher, B. L.: Statistical downscaling using localized constructed analogs (LOCA), Journal of Hydrometeorology, 15, 2558–2585, 2014.

Pierce, D. W., Kalansky, J. F., and Cayan, D. R.: Climate, drought, and sea level rise scenarios for California's fourth climate change assessment, California Energy Commission and California Natural Resources Agency, 2018.

Rao, K., Williams, A. P., Diffenbaugh, N. S., Yebra, M., and Konings, A. G.: Plant-water sensitivity regulates wildfire vulnerability, Nature Ecology & Evolution, https://doi.org/10.1038/s41559-021-01654-2, 2022.

Rempe, D. M. and Dietrich, W. E.: Direct Observations of Rock Moisture, a Hidden Component of the Hydrologic Cycle, Proceedings of the National Academy of Sciences, 115, 2664–2669, https://doi.org/10.1073/pnas.1800141115, 2018.

Restaino, C., Young, D. J., Estes, B., Gross, S., Wuenschel, A., Meyer, M., and Safford, H.: Forest structure and climate mediate drought-induced tree mortality in forests of the Sierra Nevada, USA, Ecological Applications, 29, e01 902, 2019.

Rungee, J., Bales, R., and Goulden, M.: Evapotranspiration response to multiyear dry periods in the semiarid western United States, Hydrological Processes, 33, 182–194, 2019.

Spawn, S. A. and Gibbs, H. K.: Global Aboveground and Belowground Biomass Carbon Density Maps for the Year 2010, ORNL DAAC, Oak Ridge, Tennessee, USA, https://doi.org/10.3334/ORNLDAAC/1763, 2020.

Stocker, B. D., Tumber-Dávila, S. J., Konings, A. G., Anderson, M. C., Hain, C., and Jackson, R. B.: Global patterns of water storage in the rooting zones of vegetation, Nature geoscience, 16, 250–256, 2023.

Stovall, A. E., Shugart, H., and Yang, X.: Tree height explains mortality risk during an intense drought, Nature Communications, 10, 1–6, 2019.

Swain, D. L., Langenbrunner, B., Neelin, J. D., and Hall, A.: Increasing Precipitation Volatility in Twenty-First-Century California, Nature Climate Change, 8, 427–433, https://doi.org/10.1038/s41558-018-0140-y, 2018.

Tague, C. L. and Moritz, M. A.: Plant accessible water storage capacity and tree-scale root interactions determine how forest density reductions alter forest water use and productivity, Frontiers in Forests and Global Change, 2, 36, 2019.

Thomson, A. M., Calvin, K. V., Smith, S. J., Kyle, G. P., Volke, A., Patel, P., Delgado-Arias, S., Bond-Lamberty, B., Wise, M. A., Clarke, L. E., and Edmonds, J. A.: RCP4.5: a pathway for stabilization of radiative forcing by 2100, Climatic Change, 109, 77–94, https://doi.org/10.1007/s10584-011-0151-4, 2011.

Trugman, A. T., Anderegg, L. D., Anderegg, W. R., Das, A. J., and Stephenson, N. L.: Why Is Tree Drought Mortality so Hard to Predict?, Trends in Ecology & Evolution, 36, 520–532, https://doi.org/10.1016/j.tree.2021.02.001, 2021.

Underwood, E. C., Viers, J. H., Klausmeyer, K. R., Cox, R. L., and Shaw, M. R.: Threats and biodiversity in the mediterranean biome, Diversity and Distributions, 15, 188–197, 2009.

US Forest Service: Record 129 Million Dead Trees in California, https://www.fs.usda.gov/detail/catreemortality/toolkit/?cid=FSEPRD565838, 2017a.

US Forest Service: 2014-2017 Forest Health Monitoring Program Aerial Survey Results, 2017b.

Wang-Erlandsson, L., Bastiaanssen, W. G. M., Gao, H., Jägermeyr, J., Senay, G. B., van Dijk, A. I. J. M., Guerschman, J. P., Keys, P. W., Gordon, L. J., and Savenije, H. H. G.: Global Root Zone Storage Capacity from Satellite-Based Evaporation, Hydrology and Earth System Sciences, 20, 1459–1481, https://doi.org/10.5194/hess-20-1459-2016, 2016.

Witty, J. H., Graham, R. C., Hubbert, K. R., Doolittle, J. A., and Wald, J. A.: Contributions of Water Supply from the Weathered Bedrock Zone to Forest Soil Quality, Geoderma, 114, 389–400, https://doi.org/10.1016/S0016-7061(03)00051-X, 2003.

Yang, Y., Anderson, M. C., Gao, F., Wood, J. D., Gu, L., and Hain, C.: Studying drought-induced forest mortality using high spatiotemporal

470   resolution evapotranspiration data from thermal satellite imaging, Remote Sensing of Environment, 265, 112 640, 2021.

Zhang, Y., Kong, D., Gan, R., Chiew, F. H. S., McVicar, T. R., Zhang, Q., and Yang, Y.: Coupled Estimation of 500 m and 8-Day Resolution Global Evapotranspiration and Gross Primary Production in 2002–2017, Remote Sensing of Environment, 222, 165–182, https://doi.org/10.1016/j.rse.2018.12.031, 2019.

Zhang, Z. Q., Evaristo, J., Li, Z., Si, B. C., and McDonnell, J. J.: Tritium analysis shows apple trees may be transpiring water several decades

475   old, Hydrological Processes, 31, 1196–1201, 2017.

Supporting Information: Mechanisms underlying the vulnerability of seasonally dry ecosystems to drought

Daniella M. Rempe, Erica L. McCormick, W. Jesse Hahm, Geeta Persad, Cameron Cummins, Dana A. Lapides, K. Dana Chadwick, David N. Dralle

Correspondence: Daniella M. Rempe.
E-mail: rempe@utexas.edu
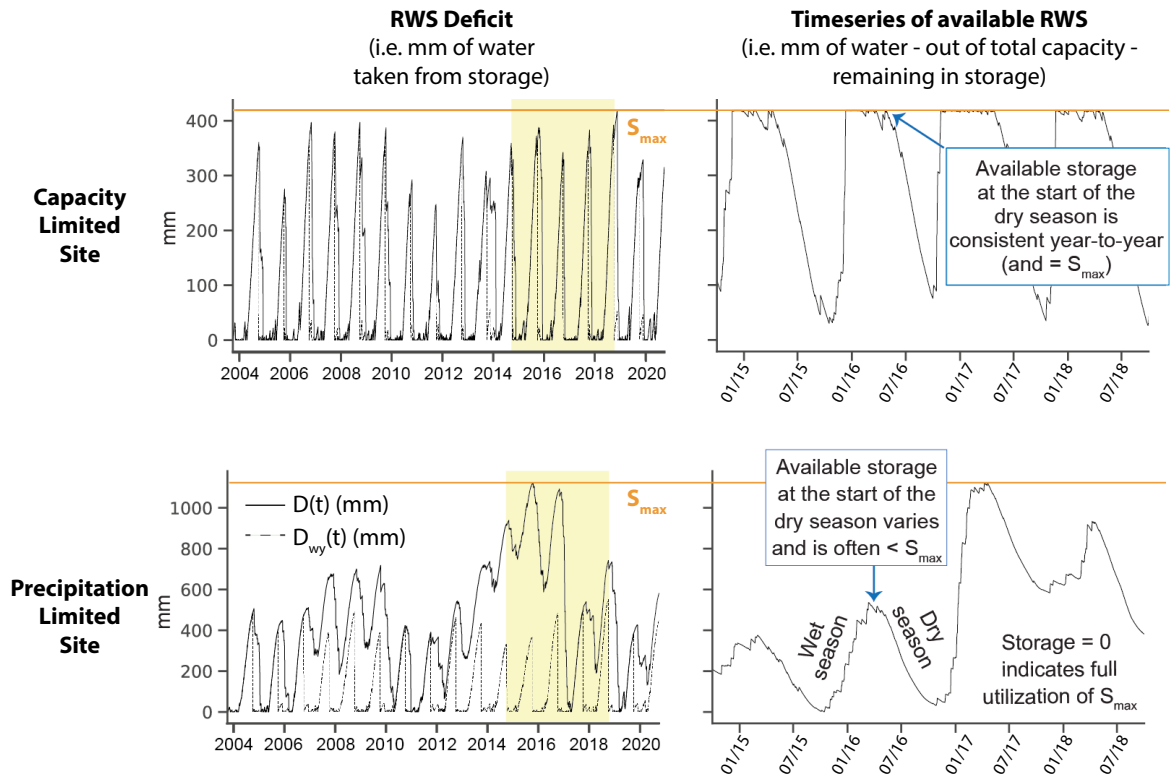
Figure S 1. Time series of deficit, $D(t)$, water year deficit, $D_{wy}(t)$, and root-water storage (RWS) from 2003 to 2020 for locations shown in Figure 1a-f. The top panel is capacity limited and the bottom panel is precipitation limited. The dashed line represents $D_{wy}(t)$ where deficits are reset to 0 at the start of each water year. Root-zone water storage capacity, S_{max}, is calculated as the $max(D(t)$ and designated by an orange line. The right panel shows timevarying root-zone water storage (RWS) at the same locations for the years 2015 to 2018 (region highlighted in yellow on left). Storage is filled by winter precipitation, with the maximum value representing S_{max}, and is depleted during the dry season.
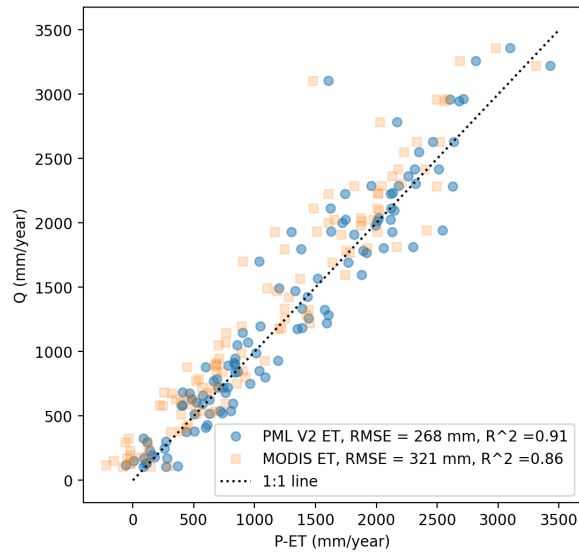
Figure S 2. Evaluation of water budget closure for seasonally dry (asynchronicity index >0.4, calculated following Feng et al. (2019)) for watersheds from the Catchment Attributes and Meteorology for Large-sample Studies (CAMELS) dataset (Newman et al., 2015). Precipitation from PRISM less evapotranspiration from PML V2 is compared to runoff from USGS streamflow for 111 North American watersheds classified as minimally impacted with an annual runoff exceeding 100 mm. RMSE and R^2 (for a 1:1 relationship) show slightly better water budget closure for the PML V2 ET dataset relative to MODIS ET. Importantly, MODIS tends to overestimate ET, which leads to larger deficits and a higher apparent storage capacity, S_{max}, and thus, the categorization of more locations as vulnerable and precipitation limited. Period of record is 2003-10-01 to 2009-10-01.

Site	Root-zone water storage capacity, S_{max} (mm)		
	Deficit calculation	Minimum field measurement	Maximum field measurement
Angelo Coast Range Reserve (ACRR)	418	126	648
Sagehorn Russell Ranch (SRR)	339	55[1]	173[1].
Rancho Venada (RV)	316	80[1]	310[1]

Table S 1. Comparison of root-zone water storage capacity, S_{max}, for field sites shown in Figure 1. Field measurements are reported in Rempe and Dietrich (2018), Hahm et al. (2020) and Hahm et al. (2022) for ACRR, SRR, and RV respectively. Minimum and maximum estimates encompass the spatial variability across the field sites. Figure 2 shows borehole locations. [1] Estimates include only bedrock component of root-zone water storage capacity and are thus a lower bound estimate. Estimates for soil water storage capacity reported by gNATSGO (Soil Survey Staff, 2019) are 50 mm and 74 mm for SRR and RV respectively.

3
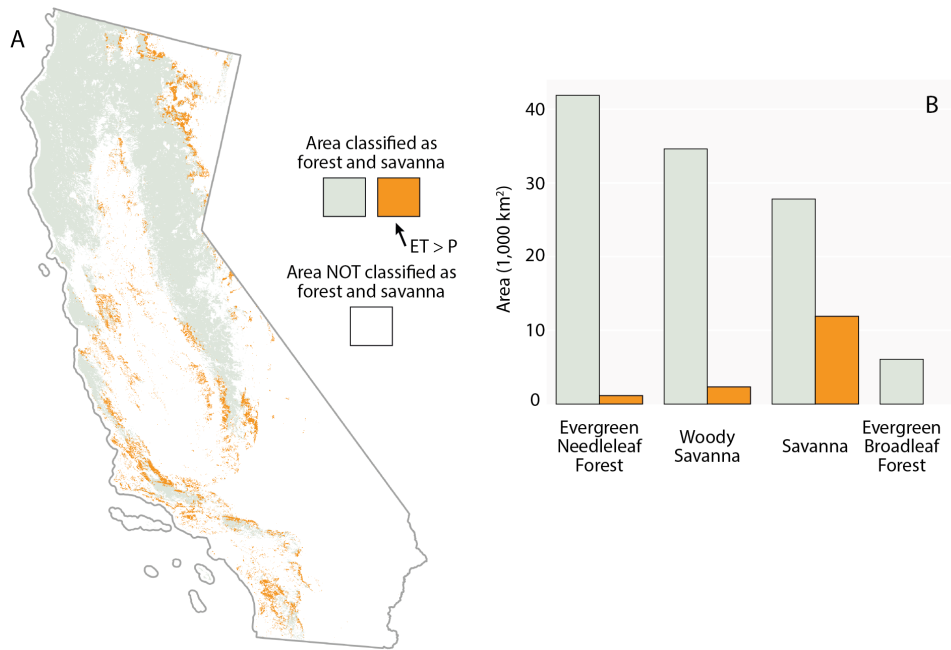
Figure S 3. (A) Locations mapped as forested or savanna (Friedl and Sulla-Menashe, 2015) where orange indicates locations which were removed because cumulative evapotranspiration exceeds cumulative precipitation (i.e. ET>P) for the years 2003 to 2020. (B) Cumulative area of woody vegetated pixels by landcover type (Friedl and Sulla-Menashe, 2015). Deciduous broadleaf forest and mixed forest are excluded from chart because they represent less than $1,00 \ km^2$ area and contain no pixels which have ET>P. All presented data in this study (with the exception of biomass Spawn and Gibbs (2020); Spawn et al. (2020), forest mortality (Service, 2017a, b), and bedrock water storage capacity (McCormick et al., 2021)) were accessed via the Google Earth Engine (GEE) (Gorelick et al., 2017) Python application programming interface (API). We used GEE and the Rasterio (Gillies et al., 2013–), scipy (Virtanen et al., 2020), and xarray (Hoyer and Hamman, 2017) Python packages to conduct analyses. All map figures were formatted in QGIS (QGIS Development Team, 2021).
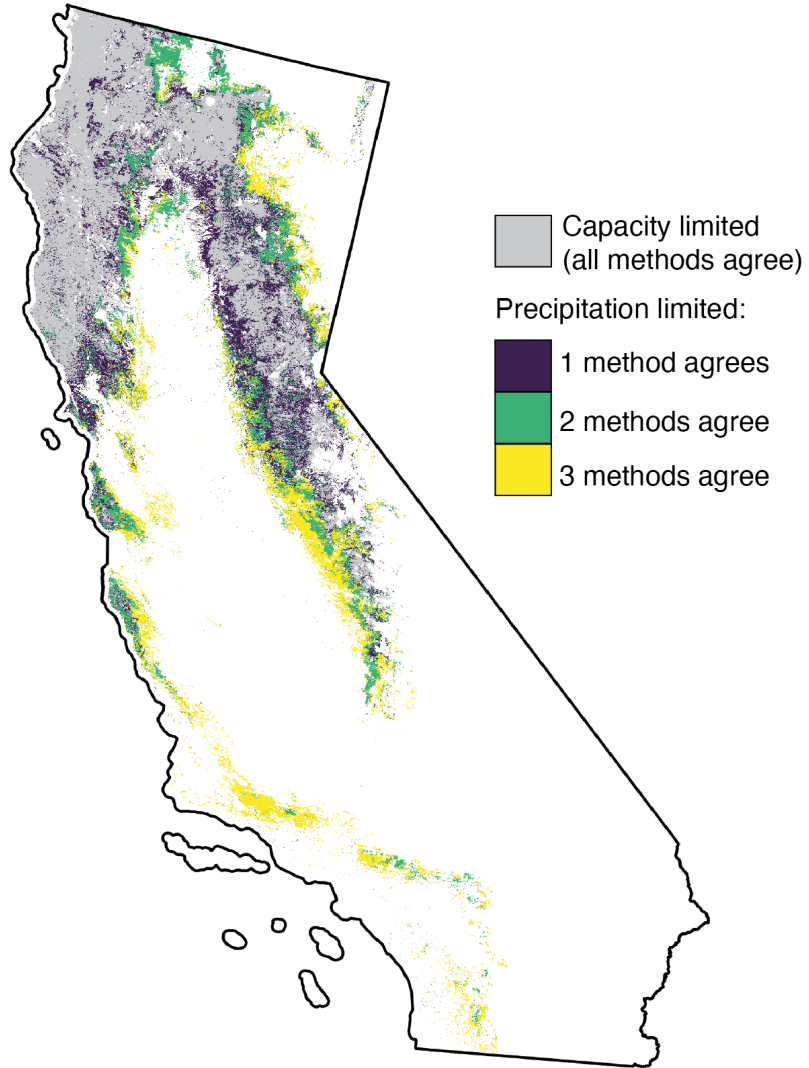
Figure S 4. Agreement between the three methods for classifying the water use of woody vegetated ecosystems as precipitation limited. Colors indicate the number of methods that agree on precipitation limitation and grey represents areas where all methods agree on capacity limitation.
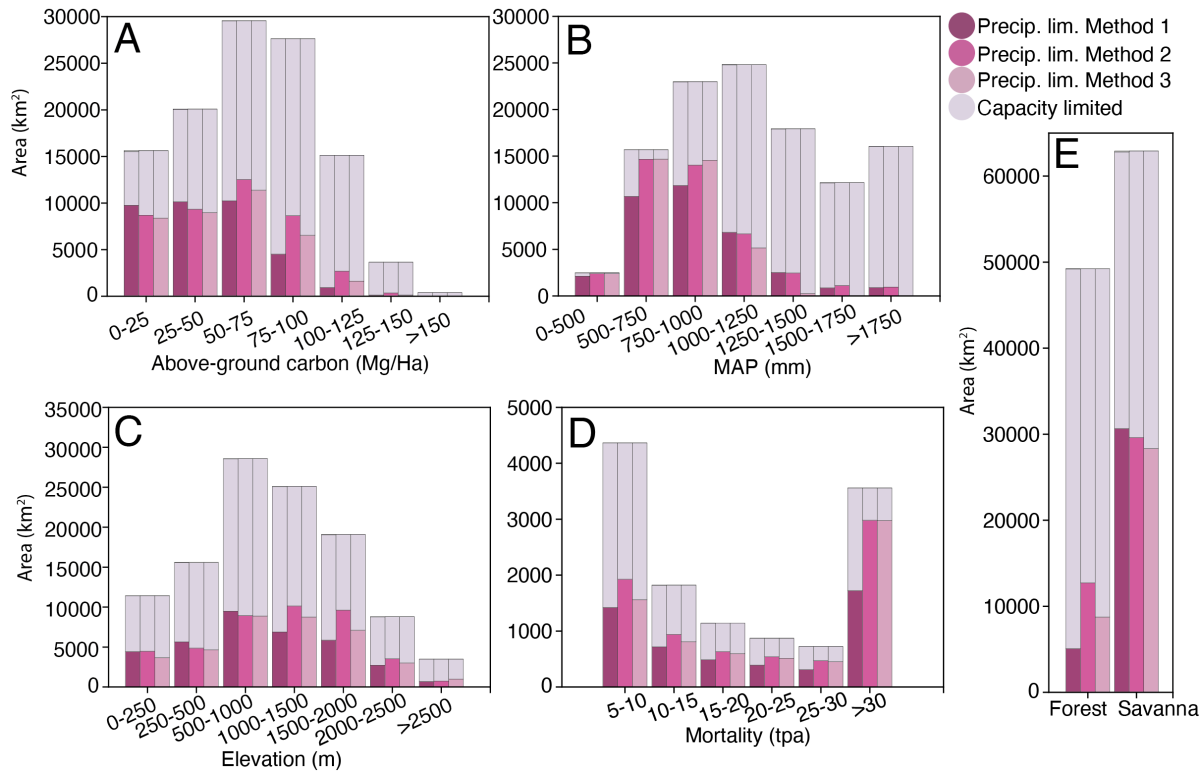
Figure S 5. The likelihood of precipitation limitation as a function of (A) above-ground carbon (Spawn and Gibbs, 2020; Spawn et al., 2020), (B) mean annual precipitation (MAP), (C) elevation, (D) tree mortality from 2014 to 2017 (US Forest Service, 2017a), and (E) landcover class (forest or savanna) (Friedl and Sulla-Menashe, 2015). The height of each bar represents the amount of area represented by each binned class (represented as bins on the x-axis). Dark pink colors indicate the area of precipitation limitation for each class and method, respectively. The likelihood of precipitation limitation (defined as the proportion of area for each class) is shown in Figure 2. Note variable y-axis limits across subplots.
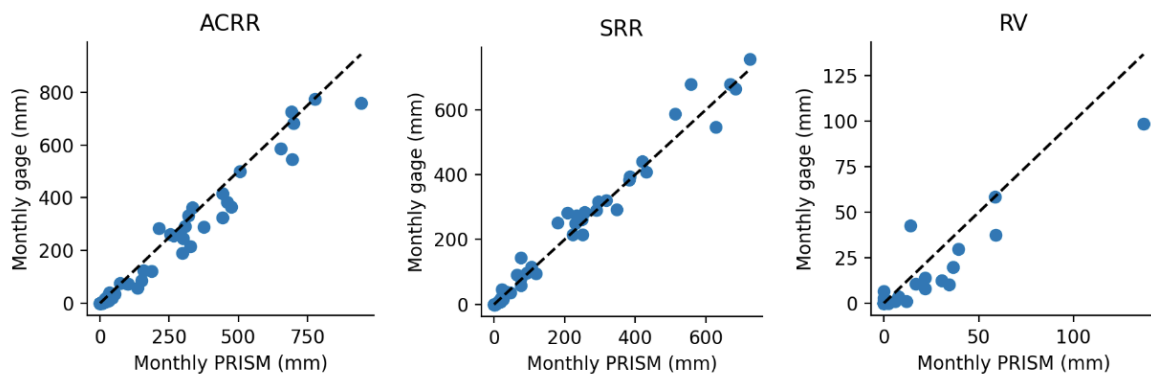
Figure S 6. Comparison of PRISM monthly precipitation to monthly precipitation totals measured via rain gauges at each of the three sites shown in Figure 1. Rain gauge data collection is described in Hahm et al., 2019 and Hahm et al., 2020.
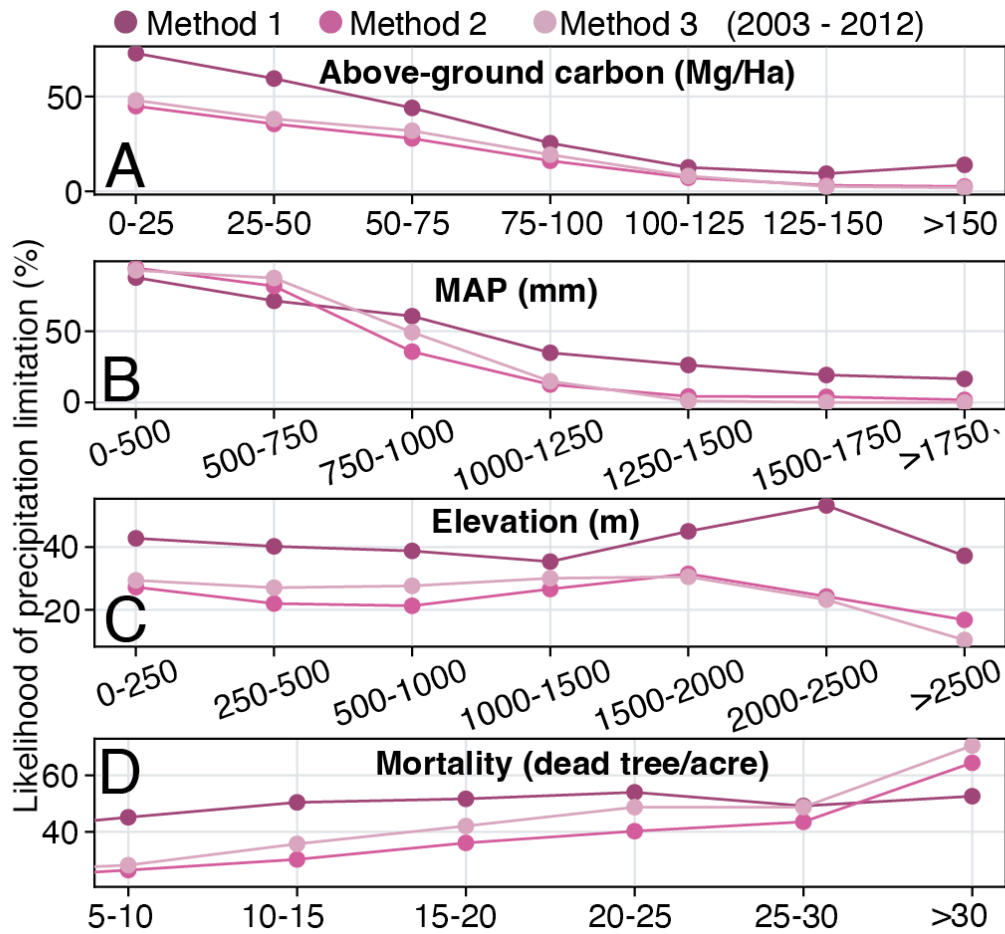
Figure S 7. The likelihood of precipitation limitation as a function of (A) above-ground carbon, (B) mean annual precipitation (MAP), (C) elevation, and (D) tree mortality from 2014-2017 (US Forest Service, 2017a) as categorized using data pre-drought data from 2003 to 2012. Likelihood is defined as the proportion of an area of a particular class (represented as bins on the x-axis) that is categorized as precipitation limited. In Figure S4, the areas of each bin are reported. This analysis is shown using the full time-series of data (2003 to 2020) in Figure 2. Note variable y-axis limits across subplots.
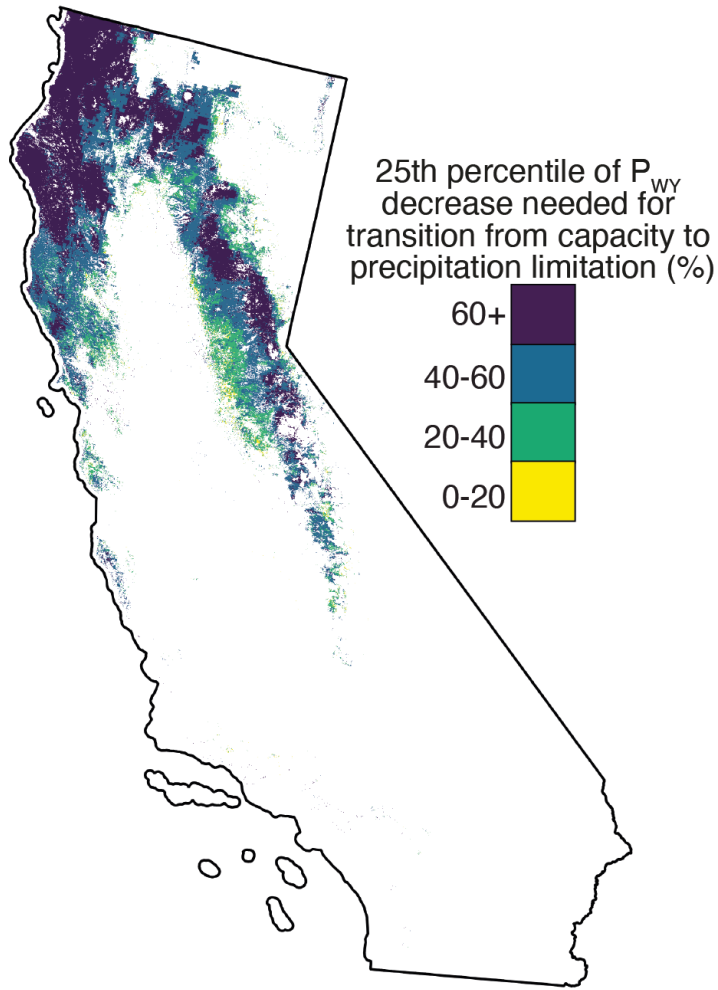
Figure S 8. Percent decrease in the 25th percentile of water year precipitation (P_{wy}) necessary to cause transition from capacity limitation to precipitation limitation according to Method 3. This map shows only areas that were categorized via Method 3 (>0% probability of $S_{max}<P_{wy}$) as capacity limited.
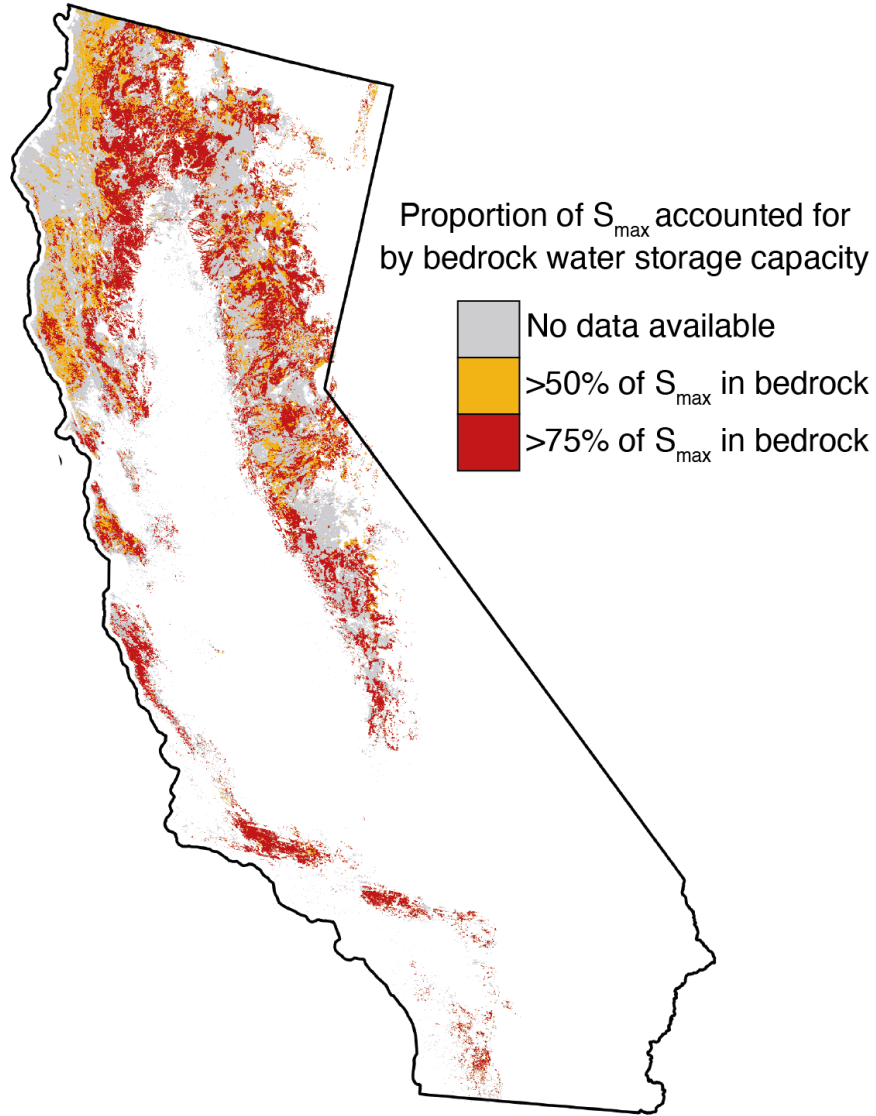
Figure S 9. The fraction of root-zone water storage capacity (S_{max}) which can be accommodated by bedrock water storage capacity. Estimates of bedrock water storage capacity from McCormick et al. (2021). Grey area represents locations included in this study which were not included in McCormick et al. (2021) and therefore do not have an estimate of bedrock water storage capacity.
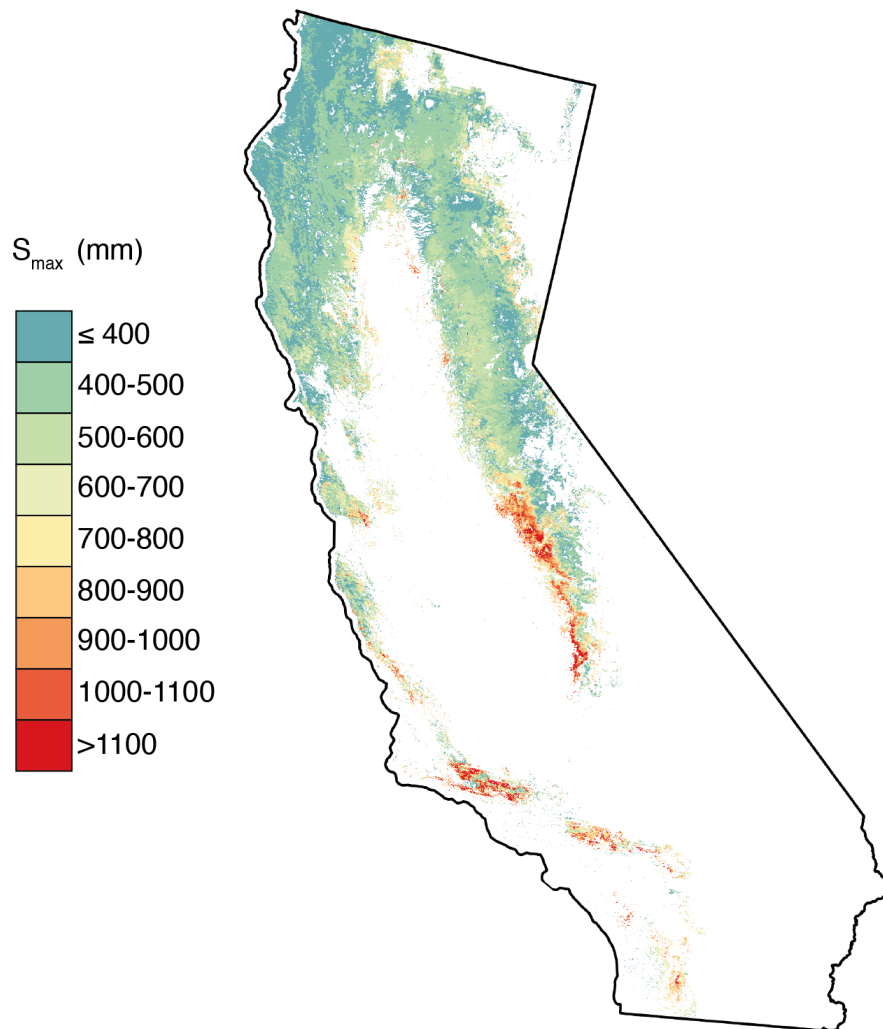
Figure S 10. Root-zone water storage capacity (S_{max}), calculated as the maximum of the root-zone water storage deficit (Figure S1, see Methods).
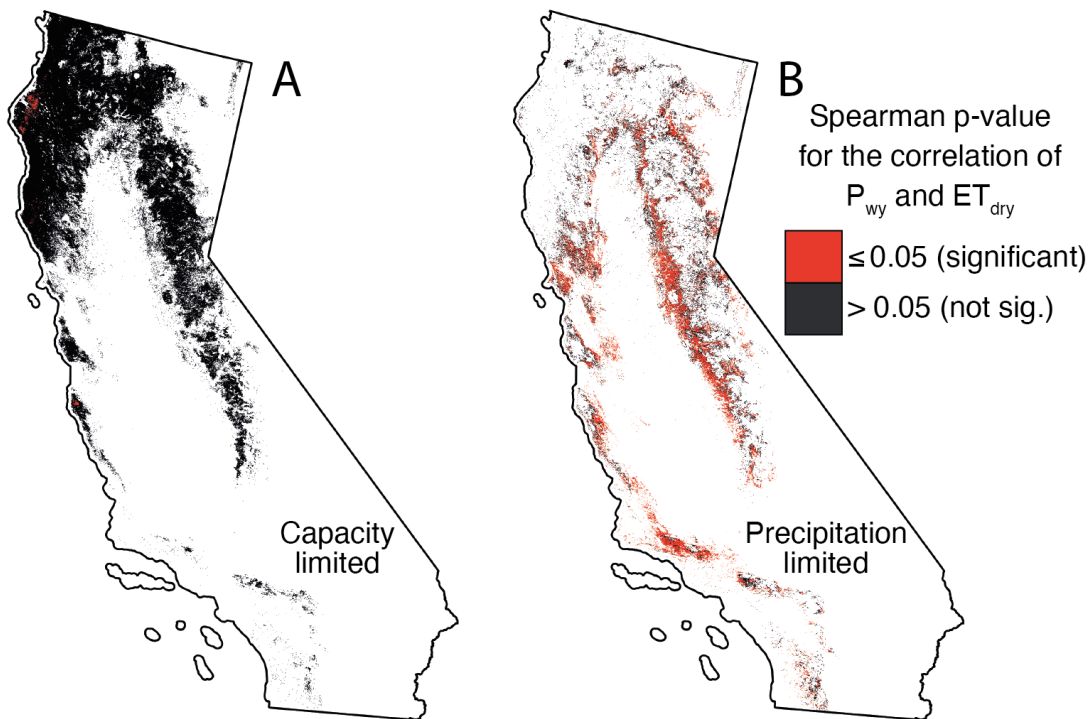
Figure S 11. Spearman p-value for the correlation between dry season evapotranspiration (ET_{dry}) and water year precipitation (P_{wy}) for regions classified as (A) storage capacity limited (B) precipitation limited according to the Spearman correlation coefficient (ρ, Method 1). Correlation coefficient (ρ) shown in Figure 1.

References

Friedl, M. and Sulla-Menashe, D.: MCD12Q1 MODIS/Terra+ aqua land cover type yearly L3 global 500m SIN grid V006 [data set], NASA EOSDIS Land Processes DAAC, 10, 2015.

Gillies, S. et al.: Rasterio: geospatial raster I/O for Python programmers, https://github.com/rasterio/rasterio, 2013–.

5 Gorelick, N., Hancher, M., Dixon, M., Ilyushchenko, S., Thau, D., and Moore, R.: Google Earth Engine: Planetary-scale geospatial analysis for everyone, Remote Sensing of Environment, https://doi.org/10.1016/j.rse.2017.06.031, 2017.

Hahm, W. J., Rempe, D. M., Dralle, D. N., Dawson, T. E., and Dietrich, W. E.: Oak Transpiration Drawn From the Weathered Bedrock Vadose Zone in the Summer Dry Season, Water Resources Research, 56, https://doi.org/10.1029/2020wr027419, 2020.

Hahm, W. J., Dralle, D. N., Sanders, M., Bryk, A. B., Fauria, K. E., Huang, M.-H., Hudson-Rasmussen, B., Nelson, M. D., Pedrazas, M. A.,
10 Schmidt, L. M., et al.: Bedrock vadose zone storage dynamics under extreme drought: consequences for plant water availability, recharge, and runoff, Water Resources Research, https://doi.org/10.1029/2021WR031781, 2022.

Hoyer, S. and Hamman, J.: xarray: N-D labeled arrays and datasets in Python, Journal of Open Research Software, 5, https://doi.org/10.5334/jors.148, 2017.

McCormick, E. L., Dralle, D. N., Hahm, W. J., Tune, A. K., Schmidt, L. M., Chadwick, K. D., and Rempe, D. M.: Widespread woody plant
15 use of water stored in bedrock, Nature, 597, 225–229, 2021.

QGIS Development Team: QGIS Geographic Information System, QGIS Association, https://www.qgis.org, 2021.

Rempe, D. M. and Dietrich, W. E.: Direct Observations of Rock Moisture, a Hidden Component of the Hydrologic Cycle, Proceedings of the National Academy of Sciences, 115, 2664–2669, https://doi.org/10.1073/pnas.1800141115, 2018.

Service, F.: Record 129 Million Dead Trees in California, https://www.fs.usda.gov/detail/catreemortality/toolkit/?cid=FSEPRD565838,
20 2017a.

Service, F.: 2014-2017 Forest Health Monitoring Program Aerial Survey Results, 2017b.

Soil Survey Staff: Gridded National Soil Survey Geographic (gNATSGO) Database for the Conterminous United States, Tech. rep., United States Department of Agriculture, Natural Resources Conservation Service, available online at /https://nrcs.app.box.com/v/soils, 2019.

Spawn, S. A. and Gibbs, H. K.: Global Aboveground and Belowground Biomass Carbon Density Maps for the Year 2010, ORNL DAAC,
25 Oak Ridge, Tennessee, USA, https://doi.org/10.3334/ORNLDAAC/1763, 2020.

Spawn, S. A., Sullivan, C. C., Lark, T. J., and Gibbs, H. K.: Harmonized global maps of above and belowground biomass carbon density in the year 2010, Scientific Data, 7, 112, https://doi.org/10.1038/s41597-020-0444-4, 2020.

Virtanen, P., Gommers, R., Oliphant, T. E., Haberland, M., Reddy, T., Cournapeau, D., Burovski, E., Peterson, P., Weckesser, W., Bright, J., van der Walt, S. J., Brett, M., Wilson, J., Millman, K. J., Mayorov, N., Nelson, A. R. J., Jones, E., Kern, R., Larson, E., Carey, C. J., Polat,
30 İ., Feng, Y., Moore, E. W., VanderPlas, J., Laxalde, D., Perktold, J., Cimrman, R., Henriksen, I., Quintero, E. A., Harris, C. R., Archibald, A. M., Ribeiro, A. H., Pedregosa, F., van Mulbregt, P., and SciPy 1.0 Contributors: SciPy 1.0: Fundamental Algorithms for Scientific Computing in Python, Nature Methods, 17, 261–272, https://doi.org/10.1038/s41592-019-0686-2, 2020.